cies much above Q band. The waveguide dimensions and resonator lengths are so small that machining tolerances become the limiting factor. It has been shown, however, that at frequencies up to Q band, the advantages of evanescent-mode filters, of lightness and compactness, and simplicity of design and construction are readily achievable.

Acknowledgment

The authors gratefully acknowledge the contribution made to this study by Dr. J. Howard and would like also to thank G. Craven for much helpful advice.

References

[1] G. Craven, "Waveguide bandpass filters using evanescent modes," *Electron. Lett.*, vol. 2, no. 7, pp. 251–252, 1966.

[2] G. Craven "Waveguide below cutoff: A new type of microwave integrated circuit," *Microwave J.*, vol. 13, no. 8, pp. 51–58, 1970.

[3] G. Craven and C. K. Mok, "The design of evanescent mode waveguide bandpass filters for a prescribed insertion loss characteristic," *IEEE Trans. Microwave Theory Tech.*, vol. MTT-19, no. 3, pp. 295–308, 1971.

[4] W. A. Edson, "Microwave filters using ghost-mode resonance," in *I.R.E. Electronic Components Conf. Proc.*, 1961, pp. 19-1–19-12.

[5] R. V. Snyder, "New application of evanescent mode waveguide to filter design," *IEEE Trans. Microwave Theory Tech.*, vol. MTT-25, pp. 1013–1021, Dec. 1977.

[6] W. W. Mumford, "Maximally-flat filters in waveguide," *Bell Syst. Tech. J.*, vol. 27, p. 684, 1948.

Extension of Levy's Large-Aperture Design Formulas to the Design of Circular Irises in Coupled-Resonator Waveguide Filters

A. JENNINGS, MEMBER, IEEE, AND R. L. GRAY

***Abstract*—This paper extends some results for waveguide irises to obtain accurate design formulas for the design of circular waveguide irises in coupled-resonator rectangular waveguide filters. Experimental results confirm the improved accuracy of the new design formulas.**

The new approach has been successfully applied to the design of a 12-GHz waveguide filter in WR90 waveguide for satellite transponder studies. Improved accuracy in the iris design enabled the filter to meet stringent group delay specifications.

I. Introduction

A waveguide coupled-resonator filter typically consists of a number of half-wavelength sections coupled via irises in the resonator walls, as illustrated in Fig. 1(a). When stringent specifications are placed on the filter, the need arises for accurate design of the irises. In the course of development of a filter for satellite transponder studies [1], existing methods of design were found to be inadequate, especially for the cases where the iris diameters are an appreciable fraction of the wavelength and the thickness t of the iris is significant.

The iris coupling is described by the equivalent circuit of Fig. 1(b) and the coupling coefficient k is expressed as

$$k = \frac{L_i}{L + L_i} \tag{1}$$

where L_i is the equivalent inductance of the iris [6].

Manuscript received November 21, 1983; revised June 1, 1984.

The authors are with Telecom Australia Research Laboratories, 762–772 Blackburn Rd., Clayton North, Melbourne, Vic. 3168, Australia

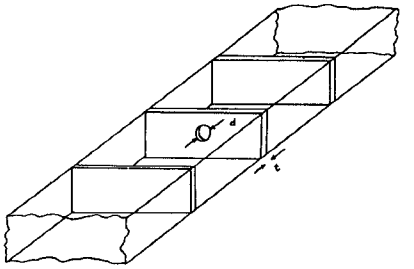

(a)

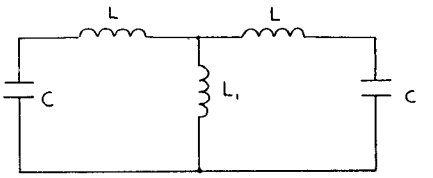

(b)

Fig. 1. (a) Iris coupling, and (b) equivalent circuit.

II. Calculation of the Iris Coupling Coefficient

For the case of small irises in thin walls, the coupling coefficient can be related to the iris diameter and the cavity dimensions in terms of simple formulas [2], [3]. Cohn [4] treats the case of large irises by employing empirical correction factors for the iris size and the wall thickness. Levy [5] has extended and applied these results to the design of multiaperture directional couplers.

McDonald [6], [7] has derived exact correction factors for wall thickness, removing the need for an empirical correction factor. Levy [9] has recently combined the results of Cohn and McDonald to give more accurate design methods for multiaperture directional couplers. In the following, Levy's results are extended to the cases of waveguide–cavity coupling and cavity–cavity coupling. This yields accurate design formulas for the irises of multicoupled waveguide filters.

The magnetic polarizability of the iris is defined as the ratio of source strength induced in the coupled cavity to incident field at the iris [2], [3]:

$$\underline{P} = -M\underline{H}_t \tag{2}$$

$\underline{P}$ magnetic dipole moment induced in the coupled cavity,
$\underline{H}_t$ tangential magnetic field incident at the iris,
M magnetic polarizability.

It can be shown [3, p. 462] that the coefficient of coupling between two cavities coupled via an end-wall iris (Fig. 2(a)) is

$$k_e = \frac{M\lambda^2 s^2}{l_1^3 ab} \tag{3}$$

λ free-space wavelength,
λ_g guide wavelength,
$l_1 = \frac{s\lambda_g}{2} s$ integer.

Similarly, the coefficient of coupling between two cavities coupled via a side-wall iris (Fig. 2(b)) is [3, p. 462]

$$k_s = \frac{M\lambda^2}{l_1 a^3 b}. \tag{4}$$

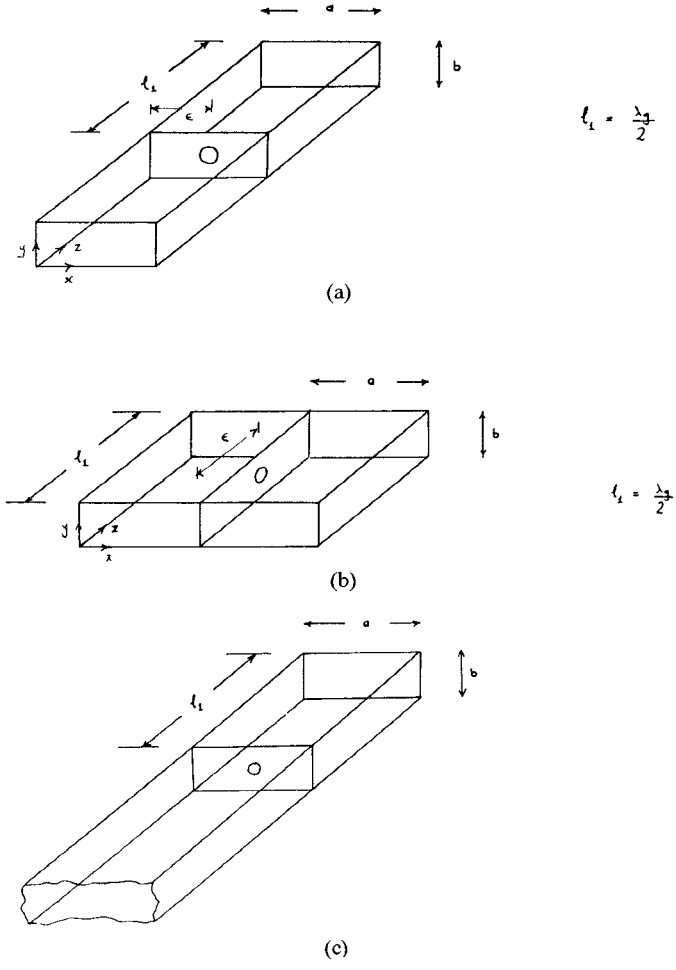

Fig. 2. (a) End-wall iris, (b) side-wall iris, and (c) input-output iris.

In the case of input and output irises (Fig. 2(c)) coupling to waveguide (i.e., the input and output ports of a multicoupled waveguide filter), the external Q of the coupled resonator is [3, p. 461]

$$Q_e = \frac{l_1^3 a^2 b^2 \lambda_g}{4\pi s^2 M^2 \lambda^2}. \tag{5}$$

Equations (3)–(5) can be used for iris design once the connection between the iris diameter d and the magnetic polarizability M has been established. In the case of a very small circular iris located in a very thin wall, the polarizability is simply [2]

$$M = d^3/6. \tag{6}$$

However, for large irises in thick walls, the coupling mechanism is more complex and several correction factors [9] must be applied. Equation (6) then becomes

$$M = c_0 c_1 c_2 d^3/6 \tag{7}$$

the correction factor c_0 takes into account the observed effect that, as the frequency of resonance of the cavity approaches the cutoff frequency of the dominant mode of the circular waveguide formed by the iris, the coupled signal increases rapidly. It is commonly approximated by the expression

$$c_0 = \frac{\tan(\pi f/2f_0)}{\pi f/2f_0}. \tag{8}$$

In the case of a circular iris $f_0 = c/\lambda_c$, where $\lambda_c = 1.705d$. While the iris-response factor is essentially an empirical correction factor, it does have some experimental [4] and theoretical [8] support. The iris-thickness correction factor c_1 has been determined exactly by McDonald [5], [6] and can be expressed as

$$c_1 = \exp\left[-\frac{2\pi At}{\lambda_c}\sqrt{1-\frac{f^2}{f_0^2}}\right]. \tag{9}$$

where $At = 1.0064t + 0.0409d$, $(t/d > 0.1)$. The field-averaging correction factor [9] takes account of the variation of the incident field $\underline{H}_t$ over the cross section of the iris. In Appendix I, new expressions are derived for c_2 in the case of cavity–cavity coupling or waveguide–cavity coupling via a circular end-wall iris

$$c_2^e \simeq 1 - \frac{1}{4}\left(\frac{\pi d}{2a}\right)^2 + \frac{1}{24}\left(\frac{\pi d}{2a}\right)^4, \qquad d/a < 0.4 \tag{10a}$$

and in the case of coupling via a circular side-wall iris

$$c_2^s \simeq 1 - \frac{1}{4}\left(\frac{\pi d}{2l_1}\right)^2 + \frac{1}{24}\left(\frac{\pi d}{2l_1}\right)^4, \qquad d/l_1 < 0.4. \tag{10b}$$

TABLE I

end-wall	side-wall
$k_e = \frac{M\lambda^2 s^2}{l_1^3 a b}$	$k_s = \frac{M\lambda^2}{l_1 a^3 b}$
$Q_e = \frac{l_1^3 a^2 b^2 \lambda_g}{4\pi s^2 M^2 \lambda^2}$	
$M = c_0 c_1 c_2 d^3/6$	$M = c_0 c_1 c_2 d^3/6$
$c_0 = \frac{\tan(\pi f/2f_0)}{\pi f/2f_0}$	$c_0 = \frac{\tan(\pi f/2f_0)}{\pi f/2f_0}$
$c_1 = \exp\left[\frac{-2\pi At}{\lambda_c}\sqrt{1-\frac{f^2}{f_0^2}}\right]$	$c_1 = \exp\left[\frac{-2\pi At}{\lambda_c}\sqrt{1-\frac{f^2}{f_0^2}}\right]$
$At = 1.0064\,t + 0.0409\,d$	$At = 1.0064\,t + 0.0409\,d$
$c_2^e = 1 - \frac{1}{4}(\frac{\pi d}{2a})^2 + \frac{1}{24}(\frac{\pi d}{2a})^4$	$c_2^s = 1 - \frac{1}{4}(\frac{\pi d}{2l_1})^2 + \frac{1}{24}(\frac{\pi d}{2l_1})^4$

III. Iris Design

Table I summarises the design formulas for circular irises. Once the coupling coefficient of the iris (or the Q_e, in the case of an input–output iris) is specified, the formulas of Table I give an expression

$$k = \Gamma(d) \tag{11}$$

for the coupling coefficient in terms of the iris diameter. Here Γ is a complicated function of the iris diameter.

In the design of the iris, an initial estimate for d is obtained from (6) and (3), (4), or (5) and the secant method [10] is then used to find the solution of the equation

$$\Gamma(d) - k' = 0 \tag{12}$$

where k' is the design value of the coupling coefficient.

IV. Example

Fig. 3 shows a 12-GHz waveguide filter designed to meet the stringent requirements of a single channel per carrier (SCPC) system for combined sound and TV broadcasting from a satellite.

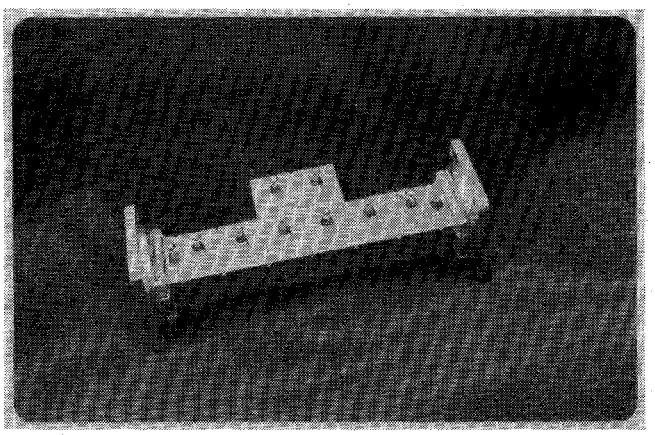

Fig. 3. 12-GHz waveguide filter.

This is an 8-resonator filter constructed in WR90 waveguide, with a single cross-coupling path for phase correction [1]. Fig. 4 shows the specifications placed on the filter.

Table II compares the measured K_1Q_e with k_1Q_e calculated from the measured iris dimensions. The measured values of coupling were obtained using a probe inserted into the two adjacent resonators. Transmission between the probes has a typical coupled tuned circuit frequency response and the frequency separation of maxima gives the coupling coefficient. Substitution of the measured physical dimensions in the various formulas enables a comparison of their accuracy. Recall that the methods used here are firmly based on the large-aperture theory of Levy [9]. While it is apparent that the present approach is an improvement over the earlier Levy [5] and Matthei, Young, and Jones [3] formulas, there still remain some anomalies. A better result would be expected for iris No. 36, which should fall within the realm of the small-aperture theory. Since the results for waveguide–cavity couplings (iris Nos. 01, 80) are significantly more in error than the cavity–cavity couplings, it would seem to indicate that a different coupling mechanism is in operation. In our case, we included aperture-adjusting screws to overcome this problem.

Despite these discrepancies, the formulas of Table I are adequate for the practical design of waveguide filters, as evidenced by the measured filter performance in Figs. 4, 5, and 6 and 7. The various models of filter were developed to test different construction practices and improve design methods. While the filters adequately meet the stopband performance and group delay performance, they do not quite meet the passband attenuation tolerance of 0.5 dB.

V. Conclusion

Levy's design formulas [9] for irises in multiaperture directional couplers have been extended to the design of circular waveguide irises in coupled-resonator waveguide filters.

Acknowledgment

The authors thank Mr. R. Owers for his careful measurements. The permission of the Director, Telecom Australia Research Laboratories, to publish this paper is gratefully acknowledged.

Appendix

The field within each cavity resonator is of the form

$$E_y = E_0 \sin\frac{\pi x}{a} \sin\frac{\pi z}{l_1}$$

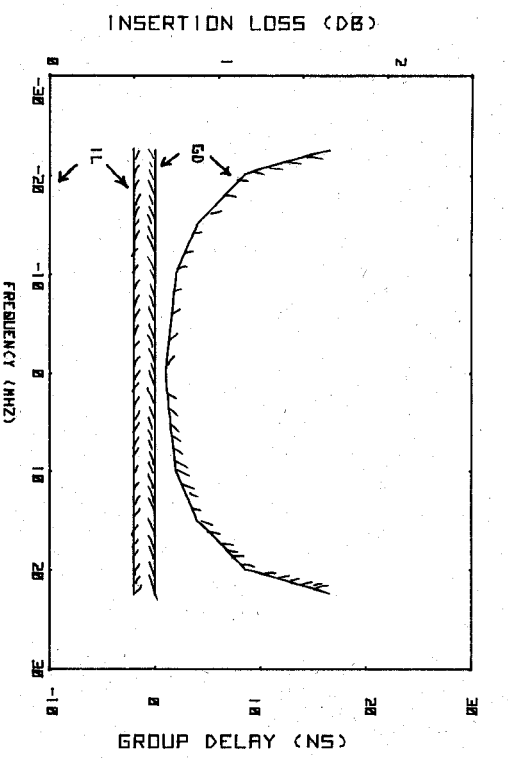

(a)

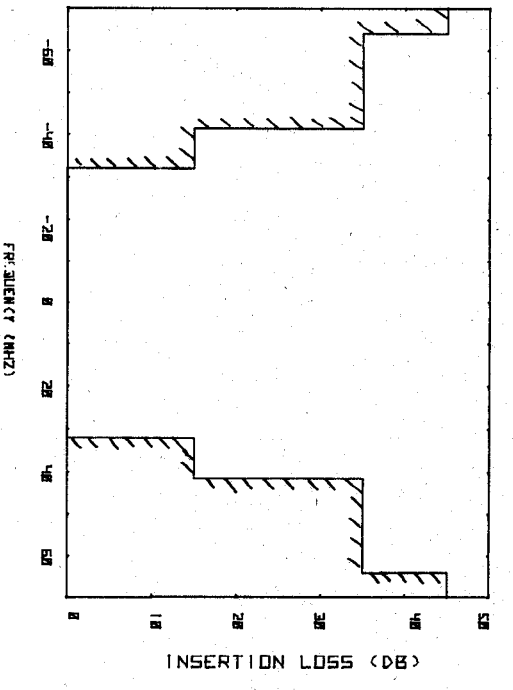

(b)

Fig. 4. (a) Filter specifications, in-band performance, (b) filter specifications, out-of-band performance.

$$H_x = -jH_0\frac{\lambda_g}{2l_1}\sin\frac{\pi x}{a}\cos\frac{\pi z}{l_1}$$

$$H_z = jH_0\frac{\lambda_g}{2a}\cos\frac{\pi x}{a}\sin\frac{\pi z}{l_1} \qquad \text{(A1)}$$

with the (x, y, z) coordinate system as defined in Fig. 2(a) and (b).

TABLE II

Iris Number	Diameter (mm)	Thickness (mm)	Measured $k \times 10^{-3}$	Table 1 $k \times 10^{-3}$ (error)	[3], [5] $k \times 10^{-3}$ (error)	Iris Type
12	4.420	1.232	4.166	3.990 (-1.48%)	4.792 (+18.32%)	end-wall
23	4.008	1.219	2.816	2.663 (-5.47%)	3.159 (+12.14%)	end-wall
34	4.839	1.303	2.325	2.268 (-2.44%)	2.254 (-3.13%)	side-wall
45	3.741	1.227	2.025	1.964 (-2.99%)	2.328 (+14.95%)	end-wall
56	4.839	1.300	2.350	2.273 (-3.30%)	2.254 (-4.07%)	side-wall
67	4.001	1.224	2.708	2.629 (-2.93%)	3.119 (+15.16%)	end-wall
78	4.420	1.229	4.033	3.998 (-0.87%)	4.753 (+17.85%)	end-wall
36	2.769	1.224	0.442	0.505 (+14.34%)	0.597 (+35.16%)	end-wall

Iris Number	Diameter (mm)	Thickness (mm)	Measured Q_e	Table 1 Q_e (error)	[3], [5] Q_e (error)	Iris Type
01	8.014	1.234	216	198.45 (-8.12%)	131.98 (-38.89%)	end-wall
80	8.014	1.232	242	198.06 (-18.16%)	131.72 (-45.57%)	end-wall

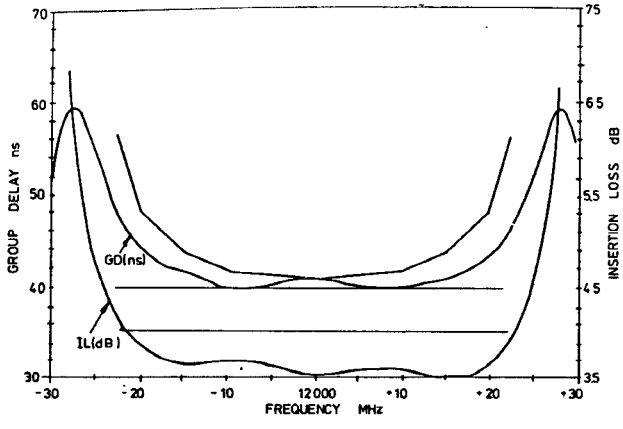

Fig. 5. Measured performance—Model 5.

The field-averaging factor c_2 is defined [9]

$$c_2 = \frac{\iint_s |\underline{H}_t|^2 \, ds}{\iint_s |\underline{H}_t(\epsilon)|^2 \, ds} \tag{A2}$$

where $\underline{H}_t$ is the incident field at the iris, $\underline{H}_t(\epsilon)$ is the incident field at the center of the iris, and S is the cross section of the iris. Fig. 2(a) shows the case of end-wall coupling.

At the iris, $\underline{H}_t$ consists entirely of the H_x component, and since the aperture is located at $z = l_1$

$$\Rightarrow H_x = -jH_0 \frac{\lambda_g}{2l_1} \sin \frac{\pi x}{a}$$

$$\Rightarrow c_2^e = \frac{\iint_s \sin^2 \pi x/a \, ds}{\iint_s \sin^2 \frac{\pi \epsilon}{a} \, ds}. \tag{A3}$$

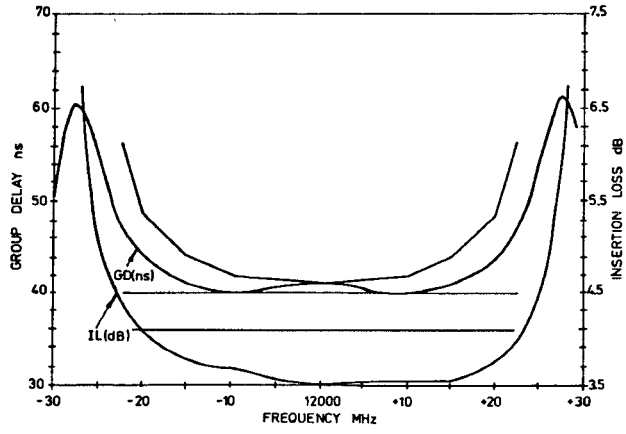

Fig. 6. Measured performance—Model 6.

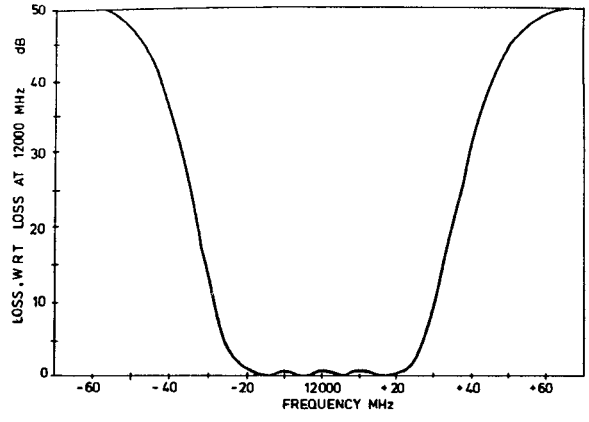

Fig. 7. Measured stopband performance.

Since $\epsilon = d/2$

$$c_2^e = \frac{4}{\pi d^2} \iint_s \sin^2 \frac{\pi x}{a} \, dx \, dy$$

$$= \frac{4}{\pi d^2} \int_{-r}^{r} \int_{\frac{a}{2} - \sqrt{r^2 - y^2}}^{\frac{a}{2} + \sqrt{r^2 - y^2}} \sin^2 \frac{\pi x}{a} \, dx \, dy$$

$$(r = d/2)$$

$$= \frac{1}{2} - \frac{4}{\pi d^2} \int_{-r}^{r} \int_{\frac{a}{2} - \sqrt{r^2 - y^2}}^{\frac{a}{2} + \sqrt{r^2 - y^2}} \frac{1}{2} \cos \frac{2\pi x}{a} \, dx \, dy$$

$$= \frac{1}{2} + \frac{4}{\pi d^2} \int_{-r}^{r} \frac{a}{2\pi} \sin \frac{2\pi}{a} \sqrt{r^2 - y^2} \, dy. \tag{A4}$$

Now, examining the remaining integral

$$\frac{2a}{\pi^2 d^2} \int_{-r}^{r} \sin\left(\frac{2\pi}{a} \sqrt{r^2 - y^2} \right) dy = \frac{4a}{\pi^2 d^2} \int_{0}^{r} \sin\left(\frac{2\pi}{a} \sqrt{r^2 - y^2} \right) dy$$

and since $\sin x = \sum_{k=0}^{\infty} (-1)^k (x^{2k+1}/(2k+1)!)$, the integral can be expressed

$$\frac{4a}{\pi^2 d^2} \int_0^r \sum_{k=0}^{\infty} (-1)^k \frac{\left(\frac{2\pi}{a} \sqrt{r^2 - y^2} \right)^{2k+1}}{(2k+1)!} \, dy$$

$$= \frac{4a}{\pi^2 d^2} \sum_{k=0}^{\infty} \frac{(-1)^k}{(2k+1)!} \int_0^r \left[\frac{2\pi}{a} \sqrt{r^2 - y^2} \right]^{2k+1} dy. \tag{A5}$$

In most cases, the iris diameter is limited in size, and hence

only the first few terms of this series need be evaluated.

$$\frac{4a}{\pi^2 d^2}\int_0^r \sin\left(\frac{2\pi}{a}\sqrt{r^2-y^2}\right)dy = \frac{4a}{\pi^2 d^2}\left[\frac{\pi^2 r^2}{2a} - \frac{\pi^4 r^4}{4a^3} + \frac{\pi^6 r^6}{23a^5} - \cdots\right] = \frac{1}{2} - \frac{1}{4}\left(\frac{\pi d}{2a}\right)^2 + \frac{1}{24}\left(\frac{\pi d}{2a}\right)^4, \quad d/a < 0.4. \quad \text{(A6)}$$

Substituting (A6) in (A4), the end-wall field-averaging correction factor is obtained

$$c_2^e = 1 - \frac{1}{4}\left(\frac{\pi d}{2a}\right)^2 + \frac{1}{24}\left(\frac{\pi d}{2a}\right)^4, \quad d/a < 0.4. \quad \text{(A7)}$$

Side-wall iris

At the iris, the incident field $\underline{H}_t$ consists entirely of the $\underline{H}_z$ component, and since the aperture is located at $x = 0$

$$H_z - jH_0\frac{\lambda g}{2a}\sin\frac{\pi z}{l_1}. \quad \text{(A8)}$$

Substituting in (A1), it is readily shown that when $\epsilon = l_{1/2}$

$$c_2^s = 1 - \frac{1}{4}\left(\frac{\pi d}{2l_1}\right)^2 + \frac{1}{24}\left(\frac{\pi d}{2l_1}\right)^4, \quad d/l_1 < 0.4. \quad \text{(A9)}$$

References

[1] R. Levy, "Filters with single transmission zeros at real or imaginary frequencies," *IEEE Trans. Microwave Theory Tech.*, vol. MTT-24, pp. 172–181, Apr. 1976.

[2] H. A. Bethe, "Theory of diffraction by small holes," *Phys. Rev.*, vol. 66, pp. 163–182, Oct. 1944.

[3] G. L. Matthei, L. Young, and E. M. T. Jones, *Microwave Filters, Impedance-Matching Networks and Coupling Structures*. New York: McGraw-Hill, 1984.

[4] S. B. Cohn, "Microwave coupling by large apertures," *Proc. IRE*, vol. 40, pp. 696–699, June 1952.

[5] R. Levy, "Analysis and synthesis of waveguide multi-aperture directional couplers," *IEEE Trans. Microwave Theory Tech.*, vol. MTT-16, pp. 955–1006, Dec. 1968.

[6] N. A. McDonald, "Electric and magnetic coupling through small apertures in shield walls of any thicknesses," *IEEE Trans. Microwave Theory Tech.*, vol. 20, pp. 689–695, Oct. 1972.

[7] N. A. McDonald, "Electromagnetic coupling through small apertures," Research Report 45, Depart. Elec. Eng., University of Toronto, Toronto, Canada, May 1971.

[8] V. K. Thong, "Solutions for some waveguide discontinuities by the method of moments," *IEEE Trans. Microwave Theory Tech.*, vol. 20, pp. 416–418, June 1972.

[9] R. Levy, "Improved single and multiaperture waveguide coupling theory, including explanation of mutual interactions," *IEEE Trans. Microwave Theory Tech.*, vol. 28, pp. 331–338, Apr. 1980.

[10] A. Ralston, *A First Course in Numerical Analysis*. Tokyo: McGraw-Hill, 1965.

A Technique to Identify Electromagnetic Modes in Oversize Waveguides

Y. CARMEL, K. R. CHU, M. E. READ, V. L. GRANATSTEIN
G. FAILLON, P. BOULANGER, E. KAMMERER,
AND G. MOURIER

Manuscript received August 25, 1983; revised March 23, 1984. This work was supported in part by the U.S. Department of Energy and, concerning Thomson–C.S.F., by the French Government (DRET).

Y. Carmel and V. L. Granatstein are with the Laboratory for Plasma and Fusion Energy Studies, University of Maryland, College Park, MD 20742.

K. R. Chu and M. E. Read are with the Naval Research Laboratory, Code 4740, Washington, DC 20375.

G. Fallon, P. Boulanger, E. Kammerer, and G. Mourier are with Thomson–C.S.F., Division Tubes Electroniques, 92102 Boulange—Billancourt Cedex, France.

***Abstract*—There are problems associated with the multimode character of oversize waveguides. This paper reports on a novel, direct way to identify modes in an oversize waveguide by looking at the field map on a liquid crystal sheet inserted in the waveguide. The local temperature change in the liquid crystal due to absorbed microwave energy is translated to a color change in such a way that a map of the local power flow is observed on the sheet.**

Mode identification is very important in gyrotrons, for example, where the microwave energy generating device is subject to severe problems from mode competition.

I. Introduction

It is well known that different modes of electromagnetic waves in a waveguide have different attenuation for a waveguide of fixed size. For example, a $TE_{0,1}^0$ (transverse electric in circular guide) mode has decreasing attenuation with increasing frequency. This property is shared by all $TE_{0,n}$ modes, and, because of this property, some waves have received a good deal of attention for possible long-distance propagation of energy [1], and for low ohmic losses in resonators of microwave and millimeter-wave power sources such as gyrotrons [2]. One of the major problems in the use of $TE_{0,n}$ in circular waveguides arises because it is not the mode of lowest cutoff frequency, and therefore must always be used in a guide capable of propagating a number of modes (known as oversize guides). For the $TE_{0,1}$ mode in a circular waveguide, there are at least four other modes propagating if the $TE_{0,1}$ mode is above cutoff ($TE_{1,1}$, $TM_{0,1}$, $TE_{2,1}$). If the $TE_{0,4}$ mode is above cutoff, at least 48 modes can propagate in the guide.

The practical problems raised by the multimode character are several. In the first place, one must have a method of exciting and identifying the desired mode. This is very important in gyrotrons, for example, where the microwave-generating device is subject to severe problems from mode competition [3], [4]. Specifically, the device can oscillate in an undesired mode having a resonance frequency close to that of the desired mode. Secondly, one must guard against coupling from the desired mode, once excited, to undesired modes. Thirdly, the measurement of power propagating in an oversize waveguide by a high-order mode wave is not simple, in contrast to power measurement in the fundamental frequency which is a routine matter. There are few ways to identify the mode of propagation in an oversize waveguide, and even to measure the fractional power in each of them. A comparison of several of the measurement methods is presented in [5] and [6].

This paper report on another, direct way to identify modes by looking at the field map on a liquid crystal sheet. This technique was first suggested by G. Faillon, following a method described in the literature, especially with regard to the study of antenna patterns [7]–[10].

II. Description of the Technique

Plastic-encapsulated liquid crystal sheets are heat sensitive, and if microwave energy is absorbed by the sheet it results in local temperature change. This temperature change appears as a local color change in such a way that a map of the RF field E (more exactly of $|E|^2$ or local power flow) can be observed on the sheet. If the liquid crystal sheet is inserted in a waveguide or horn, the mode pattern will be clearly visible. This technique is especially useful in, but not limited to, oversize waveguides in which a large number of modes can propagate.

0018-9480/84/1100-1493$01.00 ©1984 IEEE